Measurement of local porosities and dielectric dispersion for a water-saturated porous medium

Espen Haslund, Bent Dahle Hansen, Rudolf Hilfer,[a] and Bjarne Nøst
Institute of Physics, University of Oslo, P.O. Box 1048, 0316 Oslo, Norway

(Received 4 October 1993; accepted for publication 18 July 1994)

The frequency-dependent conductivity and dielectric constant of a salt-water-saturated porous glass specimen have been measured. The measurements cover the full frequency range of the Maxwell–Wagner dispersion. The experimental results have been compared with the recently introduced local porosity theory and with previous theories. For the purpose of comparing with the local porosity theory experimental measurements of local porosity distributions from digitized pore space images are presented. These experimental porosity distributions are then used for a first experimental test of local porosity theory. The comparison with previous theoretical expressions for the frequency-dependent effective dielectric function shows that local porosity theory constitutes a significant improvement in the quantitative agreement.

I. INTRODUCTION

An improved understanding of transport through porous media continues to be of great interest. In recent years a steady stream of experimental investigations (many of which were motivated by problems in hydrocarbon exploration and production) has been concerned with dielectric dispersion of water-saturated porous rocks.[1–5] A particularly convenient experimental model system for the study of transport through porous rocks are sintered glass powders filled with water. In a previous study of such specimens[4] it was shown that the dielectric dispersion curves, the dielectric constant, and the formation factor versus frequency collapsed to one curve for each of them when plotted as a function of the reduced frequency ω/ω_W, which is the circular frequency ω divided by the relaxation frequency σ/ϵ of the conducting fluid with conductivity σ and permittivity ϵ. This shows that porous glass specimens filled with a conducting fluid exhibit Maxwell–Wagner dispersion caused by the random geometry of the pore space. This type of dispersion is seen also for clay-free porous rock.[2]

Many theoretical approaches have been developed to describe the dielectric response of water-saturated porous rocks (see Refs. 6–8 for reviews). Only very recently have dielectric enhancement and conductivity-porosity relationships (such as Archies law) been obtained simultaneously from a single theoretical framework called local porosity theory.[8–11]

The objective of this study is to present a first investigation into the question to what extent local porosity theory can describe the experimental observations on water-saturated sintered glass bead systems. Such an investigation requires measurement of the so-called local porosity distribution which is of central importance in the theory and represents the mathematical characterization of the random pore space geometry. Local porosity distributions have been determined previously for computer-generated pore space images.[9]

Dielectric dispersion curves for water saturated porous glass specimens exhibit an important qualitative property. At higher frequencies, $\omega/\omega_W \sim 1$, the dielectric constant increases with porosity while at lower frequencies, $\omega/\omega_W \sim 10^{-3}$, it decreases. This implies that the curves cross each other.[4] Local porosity theory (LPT) can accommodate this crossover in qualitative agreement with experimental observations.[8] It is therefore of interest to investigate to what extent the LPT can also give more quantitative agreement.

II. THEORETICAL EXPRESSIONS FOR THE EFFECTIVE DIELECTRIC FUNCTION

The electrical response of a material is given by its complex dielectric constant $\epsilon(\omega)$ where ω is the circular frequency of the electrical test signal. The complex dielectric constant is written in the semi-insulating (SI) system as

$$\epsilon(\omega)=\epsilon'(\omega)-i\,\frac{\sigma'(\omega)}{\epsilon_0\omega}, \tag{2.1}$$

where ϵ_0 is the vacuum permittivity and $\epsilon=\epsilon'+i\epsilon''$ and $\sigma=\sigma'+i\sigma''$ are the complex dielectric constant and the conductivity, respectively, decomposed into real and imaginary parts.

Most homogeneous materials are dispersion free below 1 GHz, i.e., ϵ' and σ' are independent of ω. This is also the case for glass (or rock) and water. The mixture of glass and water, however, shows strong dielectric dispersion below 1 GHz.

The origin of this dispersion, called the Maxwell–Wagner effect,[12,13] is the difference in conductivity of the two (or more) components of the mixture. Charges build up at the boundary between the components. This charge buildup will tend to increase the polarization and decrease the conductance of the material. Because the charge buildup is not instantaneous, the effective dielectric constant and conductivity changes with frequency. For dispersion-free

[a]Also with: Institut für Physik, Universität Mainz, Postfach 3980, 6500 Mainz, Germany and Center for Advanced Study, Norwegian Academy of Sciences, P.O. Box 7606, Skillebekk, 0205 Oslo, Norway.

 0021-8979/94/76(9)/5473/8/$6.00

components both ϵ' and σ' will have a constant high-frequency and a constant low-frequency level, corresponding to complete charge buildup (low frequency) and no charge buildup (high frequency).

Theoretically it has been shown that the effective dielectric constant ϵ_e of a two-component mixture can generally be written in the following spectral representation:[14,15]

$$\epsilon_e = \epsilon_1 \left(1 - \sum_n \frac{F_n}{s - s_n} \right), \tag{2.2a}$$

$$s = \left(1 - \frac{\epsilon_2}{\epsilon_1} \right)^{-1}, \tag{2.2b}$$

where $\epsilon_1 = \epsilon_1' - i(\sigma_1'/\epsilon_0\omega)$ and $\epsilon_2 = \epsilon_2' - i(\sigma_2'/\epsilon_0\omega)$ are the complex dielectric constants of the two components, and where F_n and s_n are the strengths and positions of abstract poles reflecting the dielectric effect of the microgeometry. Equation (2.2) applies directly to our model system of water-saturated porous glass if we, for instance, identify the dielectric constant of glass $\epsilon_G = \epsilon_G'$ ($\sigma_G = 0$) with ϵ_1, and the dielectric constant of water $\epsilon_W = \epsilon_W' - i(\sigma_W'/\epsilon_0\omega)$ with ϵ_2. In Ref. 4 one of us has shown that dispersion measurements can be used to extract the pole spectrum F_n, s_n for the composite. While the spectral representation is an exact expression for ϵ_e its abstract pole spectrum has no direct interpretation in terms of geometric features of the pore space.

On the other hand several approximate theories (or mixing formulas) for the dielectric constant of a binary mixture are based on simple geometric properties of the pore space (see Ref. 6 for a review). The most widely known are the Clausius–Mossotti (CM) approximation[6,16] and the symmetrical effective medium theory[17] (EMT). The CM approximation is given as

$$\frac{\epsilon_e - \epsilon_2}{\epsilon_e + 2\epsilon_2} = f_1 \frac{\epsilon_1 - \epsilon_2}{\epsilon_1 + 2\epsilon_2}, \tag{2.3}$$

and the EMT approximation as

$$f_1 \frac{\epsilon_1 - \epsilon_e}{\epsilon_1 + 2\epsilon_e} + f_2 \frac{\epsilon_2 - \epsilon_e}{\epsilon_2 + 2\epsilon_e} = 0, \tag{2.4}$$

where ϵ_1 and ϵ_2 are the complex dielectric constants and f_1 and f_2 are the volume fractions of the components 1 and 2. If as before one identifies component 2 with the the pore-water and component 1 with the rock matrix then $f_2 = \bar{\phi}$ and $f_1 = (1 - \bar{\phi})$ where $\bar{\phi}$ is the bulk porosity. Note that contrary to EMT the CM equation is not invariant under interchange of ϵ_1 and ϵ_2.

More recently Sen and co-workers have derived expressions based on a self-similar model of the pore space. Their equation for ϵ_e is identical to the so-called differential effective medium theory (DEMT). It reads[7]

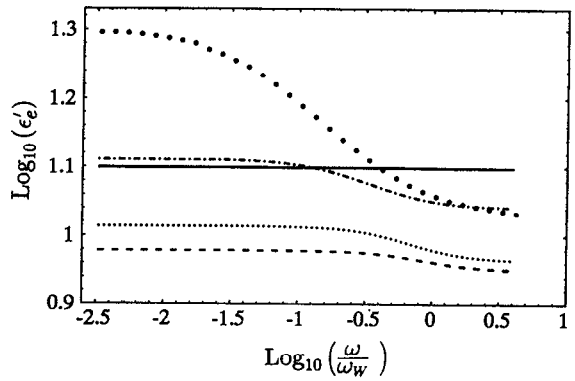

FIG. 1. Comparison of the simple approximations with the experimentally determined dielectric constant. The solid circles correspond to the experimental real part of the effective dielectric constant. The solid line corresponds to the CM approximation with water as matrix (component 2) and glass as the impurity (component 1) Eq. (2.3). The dashed line corresponds to the CM approximation with glass as matrix (component 2) and water as the impurity (component 1) Eq. (2.3). The dotted line corresponds to the symmetrical EMT approximation Eq. (2.4). The dotted-dashed line corresponds to the differential EMT Eq. (2.5a). The reduced frequency is the circular frequency of the electrical test signal divided by ω_W where $\omega_W = \sigma_W'/(\epsilon_0\epsilon_W')$ and where σ_W', ϵ_0, and ϵ_W' are conductivity of water, vacuum permittivity, and real part of dielectric constant of water.

$$\frac{(\epsilon_e - \epsilon_1)}{(\epsilon_2 - \epsilon_1)} \left(\frac{\epsilon_2}{\epsilon_e} \right)^{1/3} = \bar{\phi}, \tag{2.5a}$$

where ϵ_1 is the dielectric constant of rock (or glass), ϵ_2 is the complex dielectric constant of water, and $\bar{\phi}$ is the bulk porosity (volume fraction of component 2).

In Fig. 1 the real part of the effective dielectric constant found from the simple mixing formulas Eqs. (2.3), (2.4), and (2.5a) are compared with the experimental results. Solid circles are experimental results for a water-filled specimen of sintered 0.25 mm glass spheres. The specimen porosity is 10.7% and the water conductivity is 12.4 mS/m. It is obvious that these simple mixing laws are insufficient to describe the dielectric dispersion.

In an attempt to improve the agreement of Eq. (2.5a) with the experimental results the DEMT has been extended by considering ellipsoidal inclusions instead of spherical ones. In that case Sen and co-workers give the equation[7]

$$\frac{(\epsilon_e - \epsilon_1)}{(\epsilon_2 - \epsilon_1)} \left(\frac{\epsilon_2}{\epsilon_e} \right)^L = \bar{\phi} \tag{2.5b}$$

for spheroids having depolarization factor L. Equation (2.5b) assumes identical orientation for all spheroidal grains.

If the ellipsoids are restricted to be spheroids of identical shape but with isotropically distributed orientations the effective dielectric constant ϵ_e is given as the solution of the following equation:[2,18,19]

$$\frac{(\epsilon_e - \epsilon_1)}{(\epsilon_2 - \epsilon_1)} \left(\frac{\epsilon_2}{\epsilon_e} \right)^{3L(1-L)/(1+3L)} \left(\frac{(5-3L)\epsilon_2 + (1+3L)\epsilon_1}{(5-3L)\epsilon_e + (1+3L)\epsilon_1} \right)^{2(1-3L)^2/[(1+3L)(5-3L)]} = \bar{\phi}. \tag{2.6}$$

The depolarization factor L depends on the aspect ratio of the spheroids, and $\bar{\phi}$ is the bulk porosity of the specimen. L could be thought of as representing an abstract effective grain shape of the specimen and used as a free fitting parameter. Equation (2.6) is referred to as the uniform spheroid model (USM) and Eq. (2.5b) is referred to as the Sen-Scala-Cohen (SSC) model. More sophisticated extensions of the DEMT, involving a distribution of depolarization factors, would introduce more fitting parameters.

Recently a new approach to the calculation of effective transport quantities, LPT, has been proposed.[8–11] The LPT differs from previous theories mainly through its focus on a measurable geometric characterization of arbitrary porous media. The geometric characterization is not based on correlation functions but on local geometrical quantities such as local porosities ϕ. Within the LPT an arbitrary porous medium is quantitatively characterized through the local porosity distribution $\mu(\phi)$ and the local percolation probability[8] $\lambda(\phi)$. The local porosity distribution $\mu(\phi)$ is defined as the probability density to find a porosity between ϕ and $\phi+d\phi$ inside a local measurement cell. The local percolation probability $\lambda(\phi)$ is defined as the fraction of measurement cells with local porosity ϕ which are percolating. A local cell is said to be percolating if it contains a connection between two opposite faces. Geometric characterization through $\mu(\phi)$ and $\lambda(\phi)$ is different from more conventional correlation function approaches as was demonstrated recently.[9]

According to LPT the effective dielectric constant $\epsilon_e(\omega)$ is given by the following equation:

$$\int_0^1 \frac{\epsilon_C(\omega;\phi)-\epsilon_e(\omega)}{\epsilon_C(\omega;\phi)+2\epsilon_e(\omega)}\lambda(\phi)\mu(\phi)d\phi + \int_0^1 \frac{\epsilon_B(\omega;\phi)-\epsilon_e(\omega)}{\epsilon_B(\omega;\phi)+2\epsilon_e(\omega)}[1-\lambda(\phi)]\mu(\phi)d\phi=0, \tag{2.7}$$

where $\epsilon_C(\omega;\phi)$ and $\epsilon_B(\omega;\phi)$ are the dielectric constant of a conducting C and nonconducting (blocking, B) local geometry with porosity ϕ at the circular frequency ω. ϵ_C and ϵ_B are functions of ϵ_1, ϵ_2.

III. EXPERIMENTAL PROCEDURE

A. Specimen preparation and dielectric measurements

Cylindrical slugs of roughly 35 mm in diameter and 70 mm in length were prepared by sintering glass powder of spherical grains with a diameter of approximately 0.25 mm. The experimental specimens were taken from the most homogeneous region of the raw slugs as determined by x-ray tomography. They were cut and ground into cylinders with diameter 25 mm and length approximately 10 mm.

The dielectric dispersion is measured by placing the specimen into a parallel-plate capacitor. The admittance $Y(\omega)$ of an ideal parallel-plate capacitor filled with the composite material under investigation is given by

$$Y(\omega)=G(\omega)+i\omega C(\omega)=\frac{A}{h}[\sigma_e'(\omega)+i\omega\epsilon_0\epsilon_e'(\omega)] = i\omega\frac{A\epsilon_0\epsilon_e(\omega)}{h}, \tag{3.1}$$

where A and h are plate area and plate separation of the capacitor plates, and $G(\omega)$ and $C(\omega)$ are the conductance and capacitance of the equivalent parallel circuit. The effective dielectric constant $\epsilon_e'(\omega)$ and conductivity $\sigma_e'(\omega)$ are obtained from Eq. (3.1). A Hewlett-Packard 4192A low-frequency impedance analyzer is used to measure the admittance, and corrections are made for the parasitic capacitance. The full frequency range of the impedance analyzer, 5 Hz–13 MHz, is used, but the real dielectric constant can only be found down to the frequency where the electrode polarization starts to influence the measured dielectric constant. Platinized stainless-steel electrodes are employed in order to decrease the contact impedance.[20] The influence of the electrodes is modeled as a series coupling of a resistance R_p and a capacitance C_p. Assuming that C_p is much larger than the capacitance of the specimen C_s, that R_p is small, and the frequency not too low, the measured capacitance C and conductance G are given by[21]

$$C=C_s\left(1+\frac{G_s^2}{C_sC_p\omega^2}\right) \quad \text{and} \quad G=G_s, \tag{3.2}$$

where G_s is the conductance of the specimen. It should be noted that C_p has a frequency dependence of its own given approximately by Fricke's empirical law,[22] $C_p \propto \omega^{-m}$, where the exponent m depends on the electrode material.

B. Image of pore structure

Subsequent to the dielectric dispersion measurement, the 10.7% porosity specimen was filled with epoxy under vacuum and its end surfaces were ground flat. Pictures of these surfaces, showing the pore space structure, were obtained using a scanning electron microscope (SEM) at the lowest magnification (12 times). Each picture covered approximately 4.2×4.2 mm^2. Several pictures were taken to cover most of the specimen surface.

The SEM pictures were digitized by scanning the film with a resolution of 1024 by 1024 pixels corresponding to 4.1 μm/pixel. The digitized pictures were converted to black and white by choosing a grayness threshold for the pixels such that the porosity determined from the picture matched the measured porosity of the specimen.

The raw SEM picture of the pore space of the 10.7% porosity specimen made of 0.25 mm grains is shown together with the preprocessed digital image in Fig. 2. It is seen that the pore structure is relatively homogeneous on a large scale. The structure clearly has a typical length scale, namely the size of the spherical grains whose outlines may still be discerned. Note that the digitization acts as a high-frequency filter and has eliminated small scale details.

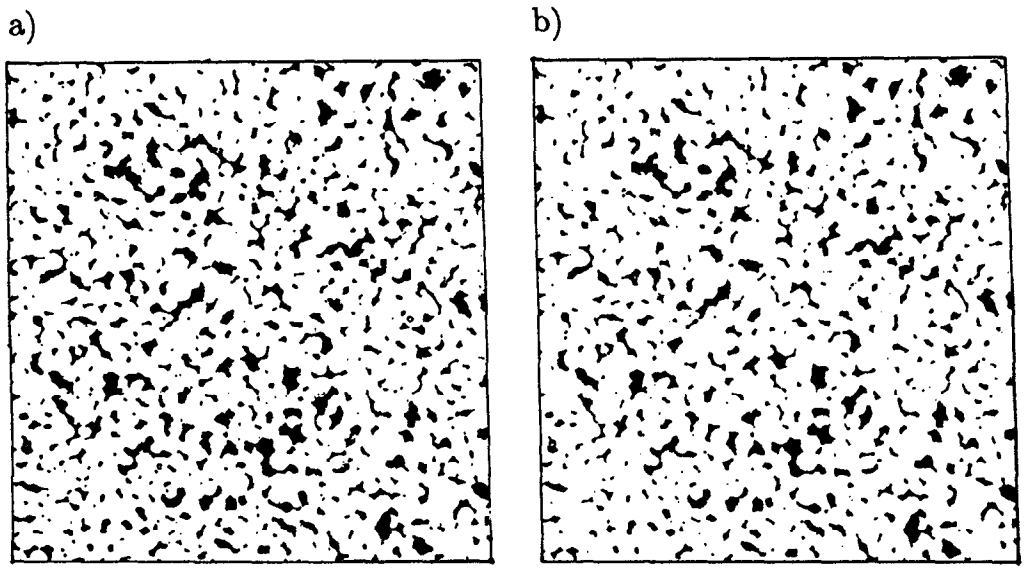

FIG. 2. SEM picture of pore space geometry. The pore space is indicated in black: (a) original SEM picture; (b) preprocessed picture where every pixel has been assigned to either pore space or matrix.

IV. POROSITY DISTRIBUTION

The local porosity distribution at length scale L, $\mu_L(\phi)$, is calculated from the preprocessed binary image of the pore space structure as described below. The program for finding the porosity distribution was written in FORTRAN, and run on a 386–20 MHz PC. A digitized picture was read into a two-dimensional integer array where the pore space was represented by 1 and the matrix by 0. The local porosity distribution at length scale L was found by placing a square measurement cell of size $L\times L$ pixels on all possible pixel positions in the picture. The local porosity at one particular position is found by summing the pixel values inside the square and dividing by L^2. The local porosities are collected into a histogram using periodic boundary conditions. Computing time was saved by adding only the new pixel values entering and subtracting the ones leaving the square each time it was moved. There will be L^2+1 possible local porosities in the range from 0 up to 1, giving a resolution in ϕ of $1/L^2$. The experimental local porosity distribution function $\mu_L(\phi)$ is obtained from the raw histogram by binning together porosities in suitably enlarged bins depending on L and then normalizing the distribution. In Fig. 3 the experimental local porosity distribution $\mu_L(\phi)$ is shown for different L values.

The two-dimensional porosity distribution found in this way is believed to be a good approximation for the three-dimensional one. The two-dimensional distribution at resolution L_2 corresponds to the three-dimensional distribution at resolution L_3. The relationship between L_2 and L_3 is given approximately by $L_2/\xi=K(L_3/\xi)^{3/2}$, where the length ξ is the typical length of the pore structure (discussed below) and the numerical constant K is close to 1.[23] As the length scale does not enter the calculation of $\epsilon(\omega)$ it can be used to fix L as suggested in Ref. 9. Here we do not follow this suggestion but instead fix L from geometric observations.[9]

In order to find the typical length ξ of the pore structure we used the two-cell porosity distribution[8] $\mu_2(\phi_1,\phi_2;R;L)$ with cells of size $L=1$. $\mu_2(\phi_1,\phi_2;R)$ is the probability of finding porosity ϕ_1 in cell 1 and at the same time porosity ϕ_2 in cell 2 at distance R from cell 1. Note that ϕ_1 and ϕ_2 can only have values zero or one as they correspond to a single pixel.

The pixel-pixel porosity autocorrelation function[8] $C(R)$, is defined via the two-cell porosity distribution by

$$C(R)=\frac{\Sigma^1_{\phi_1=0}\Sigma^1_{\phi_2=0}(\phi_1-\bar{\phi})(\phi_2-\bar{\phi})\mu_2(\phi_1,\phi_2;R)}{\bar{\phi}(1-\bar{\phi})}, \tag{4.1}$$

where $\bar{\phi}$ is the bulk porosity, ϕ_1 is porosity in cell 1, and ϕ_2 is the porosity in cell 2. The direct calculation of $C(R)$ from Eq. (4.1) is very time consuming. Therefore, a Fourier transform method was used. From the fast-Fourier-transformed

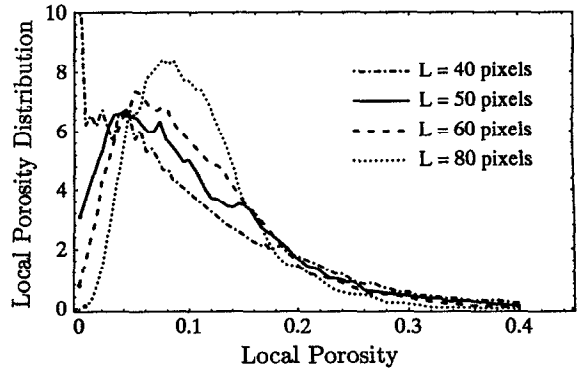

FIG. 3. The local porosity distribution function $\mu_L(\phi)$ are shown for different values of the length L of the measurement cell.

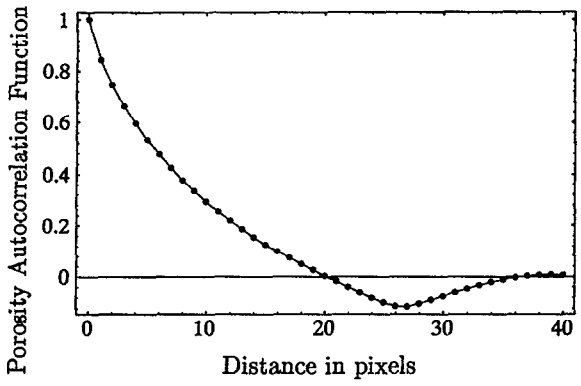

FIG. 4. The pixel-pixel porosity autocorrelation function $C(R)$ for the image in Fig. 2(b) as a function of distance in pixels.

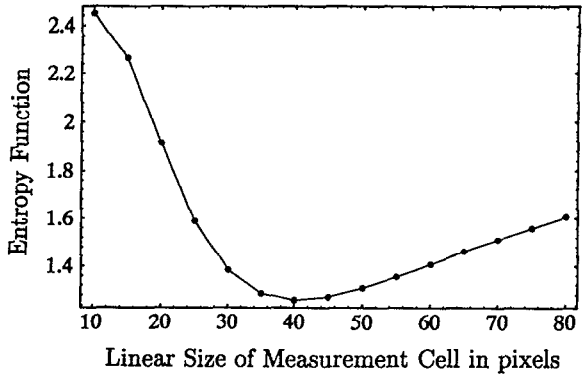

FIG. 5. Entropy function $S(L)$ as a function of the linear size in pixels of the measurement cell.

picture the power spectrum averaged over all angles was found. The porosity autocorrelation function was then obtained by Fourier inversion. We have checked that our results agree with direct calculations of $\mu_2(\phi_1,\phi_2;R)$ for small R. The porosity autocorrelation function is shown in Fig. 4.

Several methods can be used to define the correlation length ξ. A simple method is to choose ξ to be twice the distance R^* corresponding to the first minimum of $C(R)$. R^* is then a typical distance of anticorrelation, and ξ the diameter of a sphere with radius R^*. Using this method ξ was found to be about 50 pixels ($R^*=25$ pixels). Another procedure which is applicable when $C(R)$ does not have a minimum is to use the value R^* at which $C(R)$ has dropped to $1/e$. In the calculation of the dielectric response from the local porosity theory the value $\xi=50$ pixels was used.

An alternative method to find a typical length scale is to find the box size L so that the porosity distribution $\mu_L(\phi)$ contains the maximum information about the pore structure.[9] In analogy to entropy one can define a function $S(L)$ by

$$S(L)=\int_0^1 \mu_L(\phi)\ln[\mu_L(\phi)]d\phi. \tag{4.2}$$

The value L^* corresponding to the minimum of $S(L)$ is then the box size that will give the maximum information content in the porosity distribution. From the "entropy" function, $S(L)$ shown in Fig. 5, L^* is found to be 40 pixels.

V. CALCULATION OF THE DIELECTRIC CONSTANT USING LPT

In order to calculate the dielectric constant within LPT one needs to know not only the local porosity distribution as described above. In addition one also needs the probability that local geometries are percolating. This local percolation probability function $\lambda(\phi)$ can in principle be found from a three-dimensional pore-space reconstruction. In this study we have instead tried to determine $\lambda(\phi)$ indirectly by requiring that the calculated dielectric constant gives a good fit to the experimentally observed dielectric constant.

LPT divides the local geometries into two categories, percolating and nonpercolating. The percolating local geometries are modeled by a sphere of isolating material covered with a spherical shell of conducting material, while the nonpercolating local geometries are modeled by a sphere of conducting material covered with a spherical shell of isolating material. This simplification follows from the general assumption of local simplicity[8] underlying every effective medium approach. The fact that the expression used for the blocking geometry indicates isolated pore space does not imply a specific geometric model, because it represent also the accessible (but not percolating) local geometries. The expressions for the effective dielectric constant of the local geometry used in the calculations were

$$\epsilon_C(\omega;\phi)=\epsilon_W(\omega)\left(1-\frac{1-\phi}{\{1-[\epsilon_G(\omega)/\epsilon_W(\omega)]\}^{-1}-\frac{1}{3}\phi}\right), \tag{5.1a}$$

$$\epsilon_B(\omega;\phi) =\epsilon_G(\omega)\left(1-\frac{\phi}{\{1-[\epsilon_W(\omega)/\epsilon_G(\omega)]\}^{-1}-\frac{1}{3}(1-\phi)}\right). \tag{5.1b}$$

Here ϵ_C is the dielectric constant of the percolating (conducting) geometry and ϵ_B the dielectric constant of the nonpercolating (blocking) geometry. The frequency dependence enters through the dielectric constant of water $\epsilon_W(\omega)=\epsilon'_W-i(\sigma'_W/\epsilon_0\omega)$. The dielectric constant of glass $\epsilon_G(\omega)=\epsilon'_G$ is real and independent of frequency.

When the local porosity distribution and the local percolation probability are known the effective dielectric constant $\epsilon_e(\omega)$ can be found by solving Eq. (2.7) numerically. The equation has to be solved for each frequency separately, and we chose to solve for the frequencies corresponding to our dielectric measurements. The method used to find the roots of Eq. (2.7) is a fixed-point iteration technic. Because it is easier to find a good initial approximation for high frequencies we start at the high-frequency end, and work our way toward lower frequencies. For the two highest frequencies a simple weighted average of ϵ_G and ϵ_W is used as the initial value for ϵ_e. For consecutively lower frequencies the initial ϵ_e is found by extrapolating from the final result for the two closest frequencies above.

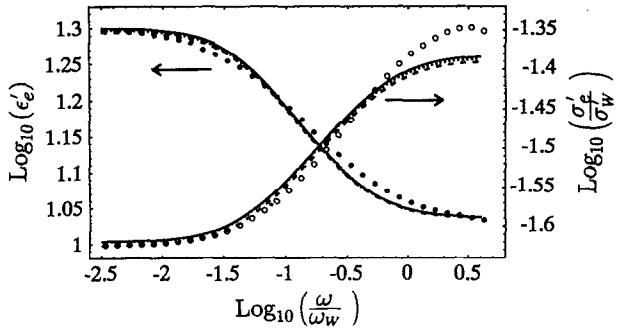

FIG. 6. Experimental and theoretical curves for the dielectric dispersion. The solid circles correspond to the experimental real part of the effective dielectric constant, and the open circles correspond to the experimental inverse formation factor (that is, the effective conductivity relative to the water conductivity). The dotted line corresponds to the dielectric dispersion calculated theoretically when a piecewise linear function with one break point is used for $\lambda(\phi)$. The solid line corresponds to a calculation using $\lambda(\phi)=\phi^{\gamma}$, and the dashed line corresponds to one with $\lambda(\phi)=\phi^{\gamma(1+C\phi)}$. See Table I for values of the fitting parameters. For the definition of reduced frequency, see Fig. 1.

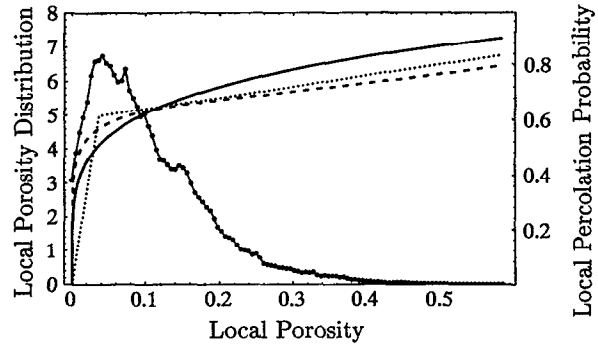

FIG. 7. Local porosity distribution and local percolation probability. The solid circles with solid lines through them correspond to the porosity distribution function $\mu_L(\phi)$, with $L=50$ pixels, used in the calculation of the theoretical curves shown in Fig. 6. The three different percolation probability functions $\lambda(\phi)$ used to obtain the theoretical curves are shown with line styles corresponding to those in Fig. 6.

The above procedure for finding the dielectric constant requires that the functions $\mu(\phi)$ and $\lambda(\phi)$ are known. The percolation probability function $\lambda(\phi)$ is, however, not known experimentally. Therefore, we tried to find shapes for $\lambda(\phi)$ that gave good fits to the dielectric measurements. The fits are obtained by minimizing the sum of the relative squared differences between the experimental values and the (λ-dependent) theoretical values of the real and imaginary part of the dielectric constant. The minimization was done on a mainframe (ND 5000) computer using the program MINUIT,[24] available from the Centre d'Etudes Recherches Nucleaires (CERN) library.

The first form for $\lambda(\phi)$ was a piecewise linear function with $\lambda(0)=0$ and $\lambda(1)=1$. The coordinates of the break points of the functions were used as fitting parameters. Second, we used an algebraic function

$$\lambda(\phi)=\phi^{\gamma}, \tag{5.2}$$

with γ as the fitting parameter. We also tried the form $\lambda(\phi)=\phi^{\gamma(1+C\phi)}$ with γ and C as fitting parameters. The last form is a rather crude attempt to introduce an exponent that varies with the local porosity.

VI. COMPARISON BETWEEN THEORIES AND EXPERIMENTS

The theoretical expressions from the CM Eq. (2.3), EMT Eq. (2.4), and DEMT Eq. (2.5a) approximations do not contain adjustable parameters, and were found above to give too small dielectric enhancement. Therefore, further comparison between theory and experiment will be restricted to the one-parameter SSC model Eq. (2.5b), the USM Eq. (2.6), and LPT Eq. (2.7). The experimentally measured dielectric dispersion curves for the 10.7% porosity specimen, for which the pore structure is seen in Fig. 2, are shown as open and solid circles in Fig. 6. The real part of the dielectric constant ϵ'_e is plotted as a function of the reduced frequency variable $\omega_r=\omega/\omega_W$, where $\omega_W \equiv \sigma'_W/(\epsilon_0\epsilon'_W)$. The effective conductivity relative to the conductivity of the salt water σ'_e/σ'_W (that is the inverse formation factor) is plotted as a function of the same reduced frequency. For this measurement $\omega_W/(2\pi)=2.82$ MHz ($\sigma'_W=12.4$ mS/m).

One can see that both the dielectric constant and the conductivity level off at low frequencies. At the intermediate frequencies there is a transition over to the high-frequency levels. The highest measurement frequency 13 MHz is slightly too low to clearly reach the high-frequency plateaux.

Figure 6 also shows the theoretical curves found from Eq. (2.7). The local porosity distribution $\mu(\phi)$ and the local percolation probabilities $\lambda(\phi)$ used as input to the theoretical expressions are shown in Fig. 7. The overall fit is good although some discrepancies are seen especially at the high-frequency end of the conductivity curve, where the experimental data however are less reliable. Note that the three different choices of the λ function (see Fig. 6) give very similar fits. The values of the fitting parameters are given in Table I.

In order not to impose any particular shape on the $\lambda(\phi)$ function we first tried to fit with a piecewise linear function for λ. Surprisingly no significant improvement in the fit was obtained by using more than one break point. The shape of

TABLE I. The table gives the three different percolation probability functions found from comparing experiments with theory (see Figs. 6 and 7). In the first column the functional form of $\lambda(\phi)$ is given. The second column gives the values of the free parameters corresponding to the best fit. The last column gives the value of the parameter $p=\int_0^1 \mu(\phi)\lambda(\phi)d\phi$.

$\lambda(\phi)$	Parameters	p
$\lambda(\phi)=\begin{cases}\left(\frac{\lambda_{bp}}{\phi_{bp}}\right)\phi, & \phi\leq\phi_{bp}\\ \lambda_{bp}+\left(\frac{1-\lambda_{bp}}{1-\phi_{bp}}\right)(\phi-\phi_{bp}), & \phi>\phi_{bp}\end{cases}$	$\phi_{bp}=0.0363$ $\lambda_{bp}=0.6155$	$p=0.589$
$\lambda(\phi)=\phi^{\gamma}$	$\gamma=0.2035$	$p=0.594$
$\lambda(\phi)=\phi^{\gamma(1+C\phi)}$	$\gamma=0.1524$ $C=3.06$	$p=0.607$

the piecewise linear function (see Fig. 7) suggests to use also an algebraic form $\lambda(\phi)=\phi^{\gamma}$, where γ is the fitting parameter. Such a choice for λ is also suggested theoretically by the central-pore model[8] for the local geometry; however, the value of $\gamma \approx 0.2$ found from the data fit is outside the range predicted by the central-pore model.[25] The best fit to the data was obtained with $\lambda(\phi)=\phi^{\gamma(1+C\phi)}$. Note that the improvement over other fits is very small.

The fact that the three different forms of $\lambda(\phi)$ give more or less the same dielectric function shows that the local porosity distribution $\mu(\phi)$ by itself imposes strong restrictions on the possible dielectric dispersion.

One of the most important aspects of the local percolation probability function $\lambda(\phi)$ is to give the correct value for low-frequency conductivity (or formation factor). The low-frequency conductivity is strongly coupled to the parameter p defined in the LPT[8] by

$$p=\int_0^1 \mu(\phi)\lambda(\phi)d\phi. \tag{6.1}$$

This parameter gives the fraction of percolating local geometries in the specimen. For the different choices of $\lambda(\phi)$ its value is found to be restricted to a very narrow range around 0.60 (see Table I for values found for p) in agreement with other independent measurements.[26]

The discrepancies between the calculated and the experimental curves can in principle be caused both by experimental error or by shortcomings of the theory. After measuring on known impedances (parallel couplings of a resistor with a capacitor), the experimental uncertainty due to the measurement instrument are seen to be smaller than the difference between the theoretical and experimental results. Discrepancies could, however, also be caused by a gradient in the water conductivity (as the water conductivity was found to show a small drift). In fact all imperfections would tend to increase the complexity of the system and therefore result in a larger dispersion and a wider frequency range of the dispersion.

Finally, the results of the LPT are compared to those of the SSC model and the USM. SSC and USM both contain the adjustable parameter L, the depolarization factor. For the local porosity theory the free parameter is the exponent γ in the algebraic λ function. Therefore, all three theoretical expressions contain exactly one free-fitting parameter. In Fig. 8 we display the experimental data together with the three theoretical fits. The LPT is seen to represent a significant improvement over both USM and the SSC model.

VII. CONCLUSION

Local porosity distributions and local percolation probabilities, as introduced in the LPT, have been used to calculate the frequency-dependent complex effective dielectric constant of a porous medium, and the results have been compared with the experimentally determined dielectric constant of the same medium.

The local porosity distribution has been determined experimentally from a digitized picture of a cross section through the pore space. The local percolation probability has been used to fit the experimental data. A good fit to experimental data is obtained for all choices of local percolation probabilities employed in the study.

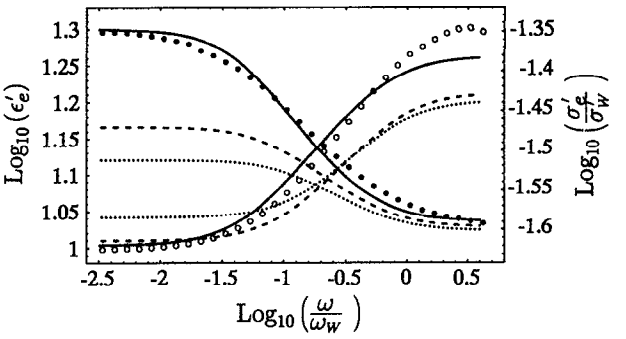

FIG. 8. Comparison between LPT and the two DEMT spheroid models (USM and SSC). The solid circles corresponds to the experimental real part of the effective dielectric constant, and the open circles give the experimental inverse formation factor (that is, the effective conductivity relative to the water conductivity). The solid line corresponds to the dielectric dispersion calculated from the LPT for the best fit with $\lambda(\phi)=\phi^{\gamma}$, $\gamma=0.2035$. The dashed line corresponds to the dielectric dispersion calculated from the USM approximation Eq. (2.6) using the best-fit value $L=0.597$ (corresponding to an aspect ratio of 2.58 for the oblate spheroids). The dotted line corresponds to the SSC model Eq. (2.6) using the best-fit value $L=0.387$ (aspect ratio 1.22). For the definition of reduced frequency see Fig. 1.

LPT was found to be a significant improvement over existing theoretical calculations of the frequency-dependent dielectric response of porous media. This investigation represents the first experimental test of the local porosity theory. Further experimental verification of the theory is, of course, necessary and in progress[26] to establish its potential as a general approach to predict the dielectric response of a porous medium. In particular a direct determination of the local percolation probability would allow a parameter-free comparison between theory and experiment.

ACKNOWLEDGMENTS

The authors are grateful to O. Milvang (Institute of Informatics) for his assistance with the digitization of the pictures. The authors are grateful to F. Boger and G. Helgesen, for discussions. One of us (R.H.) is grateful to the German–Norwegian Research and Development Program and one of us (E.H.) is grateful to the Norwegian Research Council for Science and Humanities (NAVF) for financial support.

[1] J. Ph. Poley, J. J. Nooteboom, and P. J. de Waal, Log. Anal. **19**, 8 (1978).
[2] W. E. Kenyon, J. Appl. Phys. **55**, 3153 (1984).
[3] R. J. Knight and A. Nur, Geophysics **56**, 664 (1987).
[4] I. Holwech and B. Nøst, Phys. Rev. B **39**, 12 845 (1989).
[5] C. Ruffet, Y. Gueguen, and M. Darrot, Geophysics **56**, 758 (1991).
[6] R. Landauer, in *Electrical Transport and Optical Properties of Inhomogeneous Media*, edited by J. C. Garland and D. B. Tanner, AIP conference proceedings No. 40 (AIP, New York, 1978), p. 2.
[7] P. N. Sen, C. Scala, and M. H. Cohen, Geophysics **46**, 718 (1981).
[8] R. Hilfer, Phys. Rev. B **44**, 60 (1991).
[9] F. Boger, J. Feder, T. Jøssang, and R. Hilfer, Physica A **187**, 55 (1992).
[10] R. Hilfer, Phys. Rev. B **45**, 7115 (1992).
[11] R. Hilfer, Physica A **194**, 406 (1993).
[12] K. W. Wagner, Arch. Electrotech. (Berlin) **2**, 371 (1914).
[13] R. W. Sillars, J. Inst. Electr. Eng. (London) **80**, 387 (1936).

[14] D. J. Bergman, Ann. Phys. (NY) **138**, 78 (1982).
[15] R. Fuchs, Phys. Rev. B **11**, 1732 (1975).
[16] J. C. Maxwell, *A Treatise on Electricity and Magnetism* (Dover, New York, 1954).
[17] D. A. G. Bruggeman, Ann. Phys. (Leipzig) **24**, 636 (1935).
[18] K. S. Mendelson and M. H. Cohen, Geophysics **47**, 257 (1982).
[19] P. N. Sen, Geophysics **49**, 586 (1984).
[20] C. D. Ferris, *Introduction to Bioelectrodes* (Plenum, New York, 1974).
[21] B. Nøst, B. D. Hansen, and E. Haslund, Physica Scripta **T44**, 67 (1992).
[22] H. Fricke, Philos. Mag. **14**, 310 (1932).
[23] B. Virgin and R. Hilfer (unpublished).
[24] F. James and M. Roos, Comput. Phys. Commun. **10**, 343 (1975).
[25] Note that Eq. (6.10) in Ref. 8 should read $1-\lambda=(1-a)^6+6a(1-a)^5$ and thus $\frac{2}{3}\leqslant\gamma\leqslant 1$.
[26] B. D. Hansen, E. Haslund, R. Hilfer, and B. Nøst, in *Dynamics of Small Confining Systems*, edited by J. M. Drake, J. Klafter, R. Kopelman, and D. D. Awschalon, MRS Symp. Proc. Vol. 290 (Material Research Society, Pittsburgh, PA, 1993), p. 185.